Supporting Information for:

Dielectric Effects in FeO_x-Coated Au Nanoparticles Boost Magnetoplasmonic Response: Implications for Active Plasmonic Devices

Alessio Gabbani,[1§] Elvira Fantechi,[1§] Gaia Petrucci,[1] Giulio Campo,[2] César de Julián Fernàndez,[3] Paolo Ghigna,[4] Lorenzo Sorace,[2] Valentina Bonanni,[2‡] Massimo Gurioli,[5] Claudio Sangregorio,[6,2] Francesco Pineider[1*]

[1] INSTM and Department of Chemistry and Industrial Chemistry, Università di Pisa, via G. Moruzzi 13, 56124, Pisa Italy

[2] INSTM and Department of Chemistry "U. Schiff", Università degli Studi di Firenze, via della Lastruccia 3, 50019 Sesto Fiorentino (FI), Italy

[3] CNR-IMEM, Parco Area delle Scienze 37/A, 43124 Parma, Italy

[4] Department of Chemistry, Università di Pavia, Via T. Taramelli 12, 27100 Pavia, Italy

[5] Department of Physics and Astronomy, Università degli Studi di Firenze, via G. Sansone 1, 50019 Sesto Fiorentino (FI), Italy

[6] CNR-ICCOM, Via Madonna del Piano 10, 50019 Sesto Fiorentino (FI), Italy

[§]Both authors contributed equally to this work

[‡]Present address: Elettra-Sincrotrone Trieste S.C.p.A., AREA Science Park, S.S. 14 km 163.5, Basovizza, I-34149 Trieste, Italy

[*]Corresponding author: francesco.pineider@unipi.it

1. Size distribution by TEM analysis

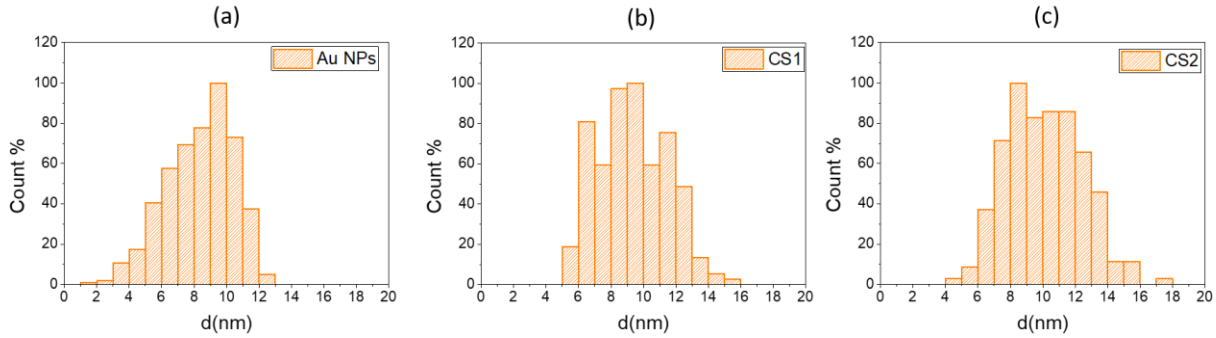

Figure S 1: Size distribution of Au NPs (a), CS 1 (b) and CS 2 (c) performed by statistic analysis of TEM images.

2. X-ray Absorption Spectroscopy pre-edge peak of reference samples γ-Fe_2O_3 and Fe_3O_4

The analysis of pre-edge peak in X-ray Absorption Spectroscopy can provide additional useful information for the structural characterization of a material. While the position of edge is determined by the binding energy of the Fe 1*s* electrons (controlled by the coulombic potential and thus influenced by the screening of valence electrons), the pre-edge peak is originated by dipole-forbidden $1s \rightarrow 3d$ transition, and its intensity is determined by deviations of the local symmetry. The different components that contribute to the pre-edge peak can be obtained by simulating the rising edge with a polynomial, and then performing a fit with by the minimum amount of Gaussian functions. In the case of Fe_3O_4, the pre-edge is constituted by two peaks, corresponding to the final states $1s^1e^4t_2^3$ and $1s^1t_{2g}^6e_g^0$, i.e. corresponding to Fe(II) in the tetrahedral crystal field (with no inversion symmetry, and therefore larger intensity) and Fe(III) in low spin configuration in the octahedral crystal field of the spinel structure, respectively. On the other hand, in γ-Fe_2O_3 the pre-edge is constituted by two peaks, corresponding to the final states $1s^1t_{2g}^4e_g^2$ and $1s^1t_{2g}^3e_g^3$, both due to Fe(III) in high spin configuration in an octahedral crystal field, respectively, and a tail at higher energy is due to long range effects involving 3*d* states in neighboring Fe sites.

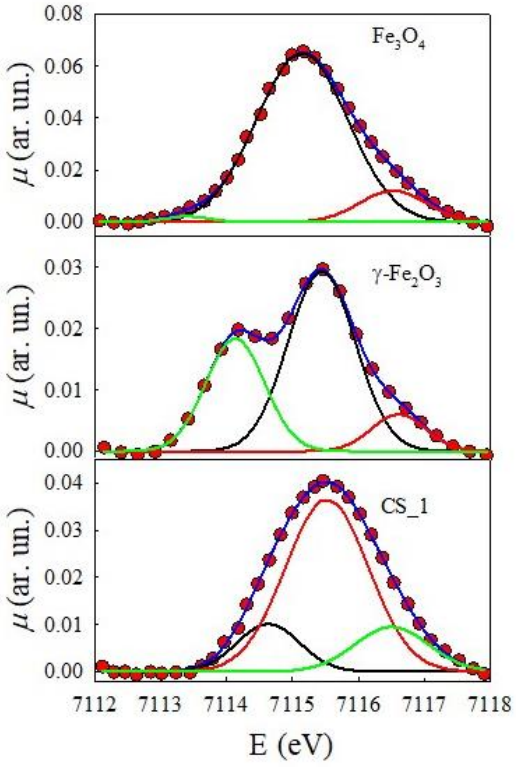

Figure S 2: Isolated pre-edge peaks of Fe_3O_4, γ-Fe_2O_3, and CS1 (top to bottom). Red circles: experimental; blue line: fit obtained by using the proper amount of Gaussian functions (black, red and green lines).

3. Electron Paramagnetic Resonance (EPR) characterization

Electron Paramagnetic Resonance (EPR) spectra were recorded at variable temperatures for a suspension of CS2 in hexane (in both frozen and in fluid phase). A broad, partially structured band centered at g=2.00, the linewidth of which clearly increases on lowering temperature, characterizes the spectra, which are of weak intensity. The resonance field position agrees with Fe^{3+} based resonance. On lowering temperature, there is no increase in the intensity of the spectrum, as would be expected if the signal were to be attributed to an isolated simple paramagnet. Further, the absence of any relevant signal at g=4.3, which is a fingerprint of the presence of isolated rhombic Fe^{3+}, indicates that there are no such active centers in the sample.[1] On the other hand, the quite large linewidth observed at all the temperatures suggests that the signal can be attributed to a disordered layer of surface spins. Indeed, the progressive broadening of the spectra on lowering temperature is a well-known phenomenon in nanostructures based on iron oxides: it arises from a reduction of the averaging effect of thermal fluctuations of the magnetization on lowering

temperature. In turn this leads to the blocking of the direction of the magnetization on the time scale of the EPR experiment, thus broadening the lines.[2,3] Spectra recorded at T > 160 K, i.e. above the melting temperature of hexane, show a clear narrowing and increase of the intensity of the signal on increasing temperature. This is due to the increased mobility of the particles which leads to a more efficient averaging of the anisotropy.[4]

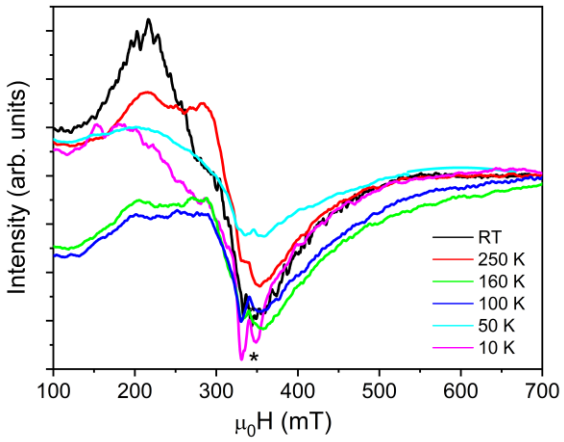

Figure S 3: X-band EPR spectra (ν = 9. 396 GHz, Mod. Amp. 6 G, Mod. Freq. = 100 KHz, Microwave power 2.08 mW) of hexane dispersions of CS2 recorded at different temperatures. The asterisk marks a spurious signal from the cavity.

4. Magnetic characterization

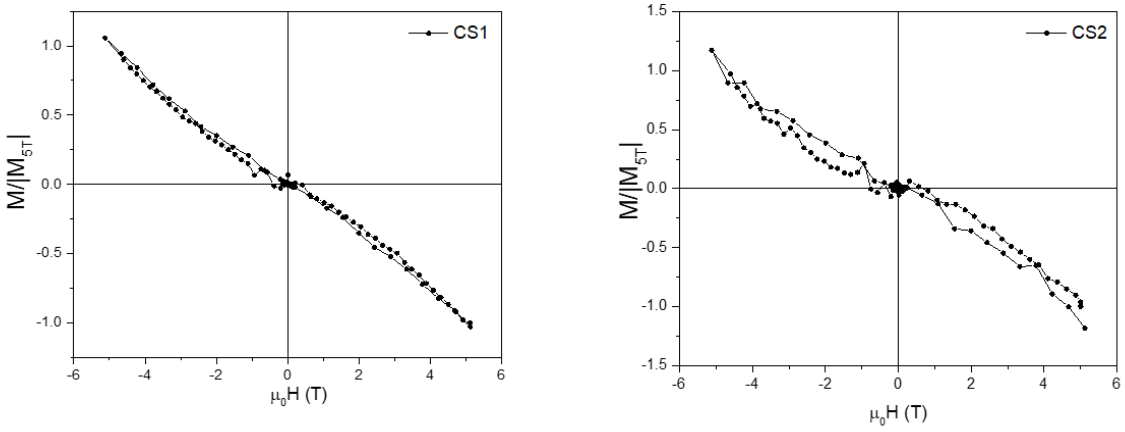

Figure S 4: M vs. H curve measured by a SQUID magnetometer at 3 K in the range ±5 Tesla.

5. Optical and magneto-optical characterization

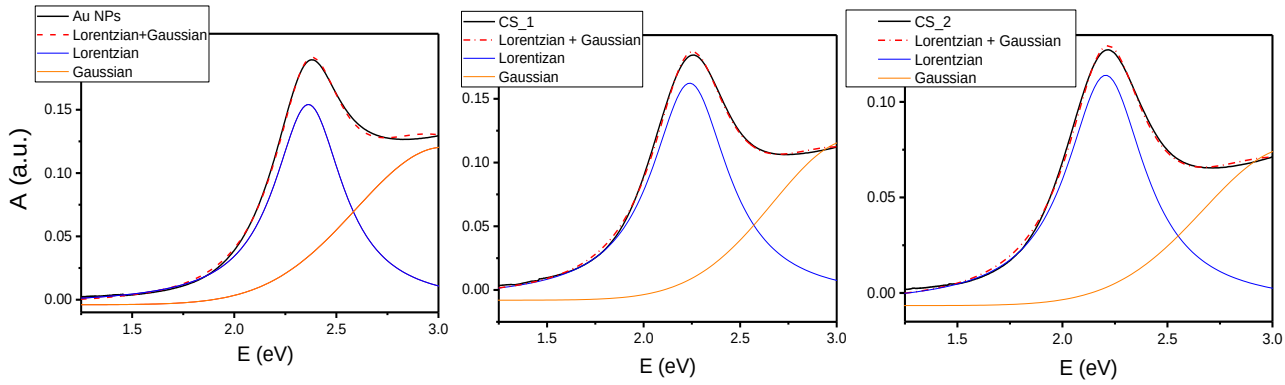

Figure S 5: Fit (red dotted line) of UV-Vis spectra (red line) of Au NPs (left), CS1 (center) and CS2 (right) using a combination of a Lorentzian (blue line) and a Gaussian (orange line) function.

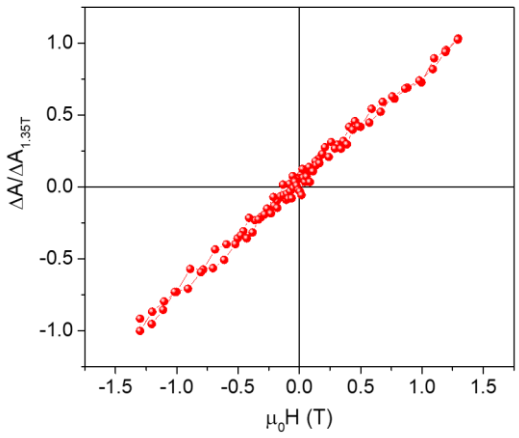

Figure S 6: Field-dependence of the MCD signal, acquired at the photon energy of the maximum of the positive MCD lobe for sample CS2 dispersed in a polystyrene matrix. The polystyrene matrix was preferred to a solvent dispersion in order to avoid the orientation of the NPs under a magnetic field application which can modify the correct probing of the magnetic properties.

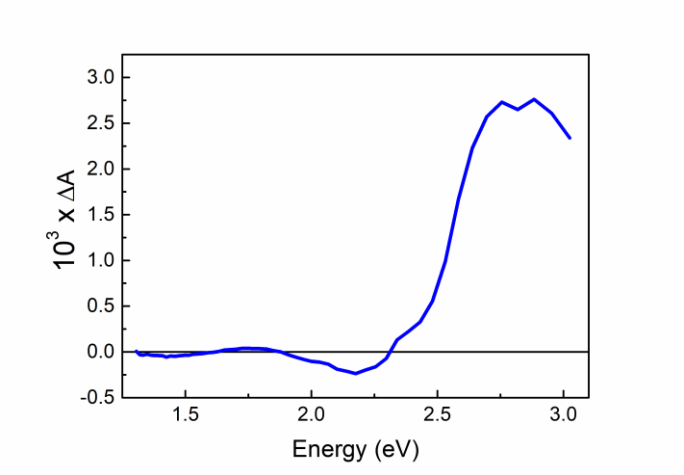

Figure S 7: Magnetic Circular Dichroism spectrum of 5 nm maghemite NPs. Data taken from reference 5.

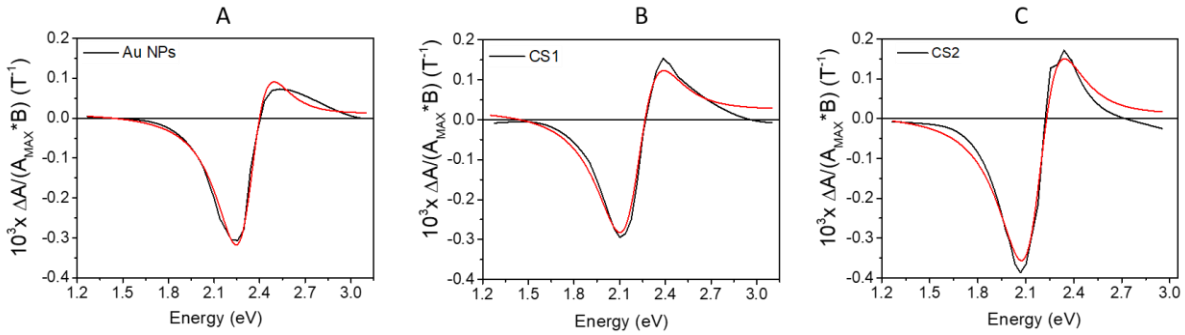

Figure S 8: Fit (red line) of MCD spectra (black line) of Au NPs of a) Au NPs, b) CS1, c) CS2 according to the fitting function described in the main text.

6. Calculation of the extinction and MCD cross section

Calculations of extinction cross section and MCD differential cross sections are performed using Matlab software, developing and executing a Matlab routine. For the case of Au NPs the field-dependent quasi-static polarizability and the related extinction cross section are calculated according to equations S1-S2.[6,7]

$$\boldsymbol{\alpha}(\boldsymbol{E},\boldsymbol{B}) = \frac{4}{3}\boldsymbol{\pi R^3}\frac{(\boldsymbol{\varepsilon}(\boldsymbol{E})-\boldsymbol{\varepsilon_m}+\boldsymbol{B}(\boldsymbol{f}(\boldsymbol{E})-\boldsymbol{f_m}))}{(\boldsymbol{\varepsilon}(\boldsymbol{E})-\boldsymbol{\varepsilon_m}+\boldsymbol{B}(\boldsymbol{f}(\boldsymbol{E})-\boldsymbol{f_m}))} \quad \text{Equation S 1}$$

$$\boldsymbol{\sigma}(\boldsymbol{E},\boldsymbol{B}) = \boldsymbol{k}\sqrt{\boldsymbol{\varepsilon_m}}\boldsymbol{imag}[\boldsymbol{\alpha}(\boldsymbol{E},\boldsymbol{B})] \quad \text{Equation S 2}$$

where B is the applied magnetic field, R is the radius of the NP, $\varepsilon(E)$ is the complex dielectric function of the metal, ε_m is the dielectric constant of the solvent (hexane in our case), while $f(E)$, and f_m are the coupling functions of the metal and the medium respectively, describing the effect of the magnetic field. The coupling function of the metal, $f(E)$, describing the effect of the magnetic field, is written according to the Drude formulation, previously reported by Gu and Kornev, and thus it considers in first approximation only the contribute of free electrons:[7]

$$f(E) = \frac{\hbar e}{m^*}\frac{E_P^2}{E}\frac{(\gamma - iE)^2}{(\gamma^2+E^2)^2}, \quad \text{Equation S 3}$$

where E_P is the plasma energy, while $f_m = 1.06\cdot10^{-6}\ T^{-1}$ is used for hexane.[6]

The extinction cross section can be obtained by employing equations S1-S2 with B=0. For spherical Au NPs, the extinction cross section for the applied field B was calculated for positive ($+B$) and negative field ($-B$) and, by subtracting the two, the MCD differential cross section per particle was obtained, which is normalized for the extinction maximum in order to be compared to the experimental MCD.

Experimental bulk dielectric functions determined by Johnson Christy are used for Au,[8] and a size correction is introduced according to Kreibig and Vollmer.[9]

To calculate the optical and MO response for CS1 and CS2 we employed the core@shell version of the dipolar quasi-static polarizability, according to Bohren and Huffman.[10] To take into account for the magnetic field effect the terms in B are introduced, in analogy with the formulation developed by Gu and Kornev.[7]

$$\boldsymbol{\alpha} = \frac{4}{3}\boldsymbol{\pi}(\boldsymbol{R}+\boldsymbol{d})^3\frac{(\boldsymbol{\varepsilon_s}-\boldsymbol{\varepsilon_m}+\boldsymbol{B}(\boldsymbol{f_s}-\boldsymbol{f_m}))(\boldsymbol{\varepsilon}+2\boldsymbol{\varepsilon_s}+\boldsymbol{B}(\boldsymbol{f}-\boldsymbol{f_s}))+(\frac{\boldsymbol{R}}{\boldsymbol{R}+\boldsymbol{d}})^3(\boldsymbol{\varepsilon}-\boldsymbol{\varepsilon_s}+\boldsymbol{B}(\boldsymbol{f}-\boldsymbol{f_s}))(\boldsymbol{\varepsilon_m}+2\boldsymbol{\varepsilon_s}+\boldsymbol{B}(\boldsymbol{f_s}-\boldsymbol{f_m}))}{(\boldsymbol{\varepsilon_s}+2\boldsymbol{\varepsilon_m}+\boldsymbol{B}(\boldsymbol{f_s}-\boldsymbol{f_m}))(\boldsymbol{\varepsilon}+2\boldsymbol{\varepsilon_s}+\boldsymbol{B}(\boldsymbol{f}-\boldsymbol{f_s}))+(\frac{\boldsymbol{R}}{\boldsymbol{R}+\boldsymbol{d}})^3(\boldsymbol{\varepsilon}-\boldsymbol{\varepsilon_s}+\boldsymbol{B}(\boldsymbol{f}-\boldsymbol{f_s}))(2\boldsymbol{\varepsilon_s}-2\boldsymbol{\varepsilon_m}+\boldsymbol{B}(\boldsymbol{f_s}-\boldsymbol{f_m}))} \quad \text{Equation S 4}$$

where R and d are the radius of the core and the shell thickness, ε and ε_s are the complex frequency-dependent dielectric functions of the core and the shell respectively, ε_m is the dielectric constant of the solvent (hexane in our case), while *f(E)*, f_s and f_m are the coupling functions of the metal, the shell and the medium respectively, describing the effect of the magnetic field. In the absence of the shell, i.e. for $\varepsilon_s=\varepsilon_m$ and $f_s=f_m$, Equation S4 is simplified to the sphere case (Equation S1).

Given the low magnetic moment of the shell at room temperature, we assumed that the coupling function of the shell is comparable with the one of the solvent ($f_s=f_m$), which is order of magnitudes lower than the coupling function of the metal, simplifying the field-dependent quasi-static polarizability to equation 1 of the main text. The dielectric function of bulk maghemite is used for the shell, taken from the experimental data of Battie *et al*.[11]

In Figure S8, the calculations of the MCD response of a simple Au NP of 8 nm were performed using the simple spherical model for the polarizability (Equation S1), changing ε_m in order to fit the experimental extinction and MCD spectra. Values of 3.06 and 3.61 were used to reproduce the MCD response of sample CS1 and CS2. The data of the calculations are plotted together with the experimental spectra in Figure S8.

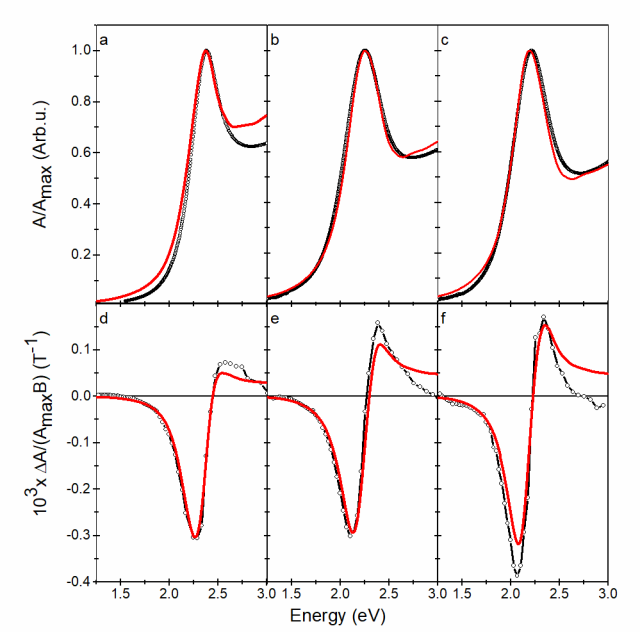

Figure S 9: Experimental (black line) and calculated (red line) extinction and MCD spectra of the three samples, Au NPs (a,d), CS1 (b,e) and CS2 (c,f). Extinction is normalized for the extinction maximum, while MCD is normalized for extinction maximum and applied magnetic field (1.4

Tesla). The spherical polarizability model is used with ε_m of 1.89 for pure Au, ε_m of 3.06 and 3.61 to reproduce the MCD of CS1 and CS2 respectively.

The magnetic field-induced energy shift is calculated according to equation 3 (main text), where the quantity $\delta\varepsilon_1/\delta E$ is computed by differentiation with respect to the photon energy of the dielectric function at the resonant energy E_0.

References:

(1) Pilbrow, J. R. *Transition Ion Electron Paramagnetic Resonance*; Oxford University Press, 1990.
(2) Sharma, V. K.; Waldner, F. Superparamagnetic and Ferrimagnetic Resonance of Ultrafine Fe3O4 Particles in Ferrofluids. *Journal of Applied Physics* **1977**, *48* (10), 4298–4302. https://doi.org/10.1063/1.323418.
(3) Raikher, Y. L.; Stepanov, V. I. Ferromagnetic Resonance in a Suspension of Single-Domain Particles. *Phys. Rev. B* **1994**, *50* (9), 6250–6259. https://doi.org/10.1103/PhysRevB.50.6250.
(4) Dobosz, B.; Krzyminiewski, R.; Koralewski, M.; Hałupka-Bryl, M. Computer Enhancement of ESR Spectra of Magnetite Nanoparticles. *Journal of Magnetism and Magnetic Materials* **2016**, *407*, 114–121. https://doi.org/10.1016/j.jmmm.2016.01.058.
(5) Campo, G.; Pineider, F.; Bonanni, V.; Albino, M.; Caneschi, A.; de Julián Fernández, C.; Innocenti, C.; Sangregorio, C. Magneto-Optical Probe for Investigation of Multiphase Fe Oxide Nanosystems. *Chem. Mater.* **2015**, *27* (2), 466–473. https://doi.org/10.1021/cm5034595.
(6) Pineider, F.; Campo, G.; Bonanni, V.; de Julián Fernández, C.; Mattei, G.; Caneschi, A.; Gatteschi, D.; Sangregorio, C. Circular Magnetoplasmonic Modes in Gold Nanoparticles. *Nano Letters* **2013**, *13* (10), 4785–4789. https://doi.org/10.1021/nl402394p.
(7) Gu, Y.; Kornev, K. G. Plasmon Enhanced Direct and Inverse Faraday Effects in Non-Magnetic Nanocomposites. *J. Opt. Soc. Am. B, JOSAB* **2010**, *27* (11), 2165–2173. https://doi.org/10.1364/JOSAB.27.002165.
(8) Johnson, P. B.; Christy, R.-W. Optical Constants of the Noble Metals. *Physical review B* **1972**, *6* (12), 4370.
(9) Kreibig, U.; Vollmer, M. *Optical Properties of Metal Clusters*; Springer-Verlag: Berlin, 1995.
(10) Bohren, C. F.; Huffman, D. R. *Absorption and Scattering of Light by Small Particles*; Wiley: New York, 1983.
(11) Battie, Y.; Stchakovsky, M.; Neveu, S.; Jamon, D.; Garcia-Caurel, E. Synthesis and Study of γ-Fe $_2$ O $_3$ and CoFe $_2$ O $_4$ Based Ferrofluids by Means of Spectroscopic Mueller Matrix Ellipsometry. *Journal of Vacuum Science & Technology B* **2019**, *37* (6), 062929. https://doi.org/10.1116/1.5121286.